High-sensitivity three-mode optomechanical transducer

C. Zhao, Q. Fang, S. Susmithan, H. Miao, L. Ju, Y. Fan, and D. Blair
School of Physics, The University of Western Australia, 35 Stirling Highway, Nedlands, Western Australia, 6009, Australia

D. J. Hosken, J. Munch, and P. J. Veitch
Department of Physics, The University of Adelaide, Adelaide, South Australia, 5005, Australia

B. J. J. Slagmolen
Centre for Gravitational Physics, The Australian National University, Canberra, 0200, Australia
(Received 19 June 2011; published 16 December 2011)

Three-mode optomechanical interactions have been predicted to allow the creation of very high sensitivity transducers in which very strong optical self-cooling and strong optomechanical quantum entanglement are predicted. Strong coupling is achieved by engineering a transducer in which both the pump laser and a single signal sideband frequency are resonantly enhanced. Here we demonstrate that very high sensitivity can be achieved in a very simple system consisting of a Fabry-Perot cavity with CO_2 laser thermal tuning. We demonstrate a displacement sensitivity of $\sim 1 \times 10^{-17}$ m/$\sqrt{\text{Hz}}$, which is sufficient to observe a thermally excited acoustic mode in a 5.6 kg sapphire mirror with a signal-to-noise ratio of more than 20 dB. It is shown that a measurement sensitivity of $\sim 2 \times 10^{-20}$ m/$\sqrt{\text{Hz}}$ limited by the quantum shot noise is achievable with optimization of the cavity parameters.

DOI: 10.1103/PhysRevA.84.063836 PACS number(s): 42.25.Fx, 07.60.Ly, 42.50.Wk

I. INTRODUCTION

Optomechanical coupling provides a means of studying the quantum behavior of macroscopic mechanical degrees of freedom and also enables high-sensitivity probes for quantum-noise-limited measurements [1]. Experiments have demonstrated optical cooling of mechanical oscillators [2]. Theoretical studies have focused on the creation of quantum entanglement of mechanical and optical degrees of freedom for quantum information [3–6] and on using such systems for probing mechanical energy quantization [7,8]. Recently, a cryogenic 10 MHz micromechanical oscillator has been cooled to its quantum ground state using sideband cooling [9]. On the kilometer scale, laser interferometer gravitational-wave detectors at the Laser Interferometer Gravitational-Wave Observatory (LIGO) [10] and VIRGO project [11] have achieved a displacement sensitivity of 10^{-19} m/$\sqrt{\text{Hz}}$ at around 100 Hz, while on a small scale the high-frequency thermal noise of a mechanical oscillator has also been measured with similar sensitivity [12]. Using high displacement sensitivity and feedback cooling, a LIGO interferometer test mass has been cooled to an effective temperature of 1.4 μK [13], corresponding to an occupation number of about 200 quanta.

In most optomechanical systems to date, a single TEM_{00} optical mode is coupled to a mechanical oscillator mode. For such two-mode systems the cavity acts like a low-pass filter which filters out high-frequency signal sidebands and therefore compromises the sensitivity at high frequencies. This effect is observed in laser interferometer gravitational-wave detectors [14,15]. Minimizing thermal noise and maximizing electromechanical coupling requires minimization of the losses of both optical and mechanical modes. However, this makes the narrow-band-filtering situation even worse. A solution to this problem is to introduce a second electromagnetic mode resonant at the mechanical sideband frequency to form a three-mode optomechanical system. When the mode spacing correctly matches the acoustic mode frequency, it has been predicted that such a *three-mode* transducer can have very high sensitivity, immunity to laser noise, and require only relatively low laser power [16].

Three-mode optomechanical interactions involving pairs of optical modes were first investigated theoretically by Braginsky *et al.* [17] in the context of long-baseline gravitational-wave detectors. They showed that such interactions could induce parametric instability in the high-optical-power cavities of advanced gravitational-wave detectors through an interaction that can inject optical energy into selected acoustic modes to the point of instability. Zhao *et al.* [18] and many others [19–21] extended this analysis to include realistic-mode-shape modeling. In 2009, Zhao *et al.* [16] pointed out that three-mode interactions can be harnessed to create a general opto-acoustic parametric amplifier (OAPA), which can function as a high-sensitivity transducer with the capability of cooling a mechanical mode down to the quantum ground state. The high sensitivity arises because the single sideband signal is coherently amplified when the frequency gap is equal to the frequency of the mechanical mode. This occurs without compromising the optical power that defines the optomechanical coupling strength. Dobrindt and Kippenberg [22] confirmed this analysis in the context of a four-mode transducer using three optical modes, and discussed the experimental challenge of engineering appropriate mode gaps. The single sideband three-mode transducer system discussed here solves the engineering problem through optical design and thermal tuning, is simple to implement, and has a sensitivity similar to a four-mode system.

The mode and frequency structure of the three-mode interaction is shown in Fig. 1. The fundamental optical mode at ω_0 is scattered by the mechanical motion of the test mass at ω_m. This creates two sideband modes: one at $\omega_0 - \omega_m$ (also called

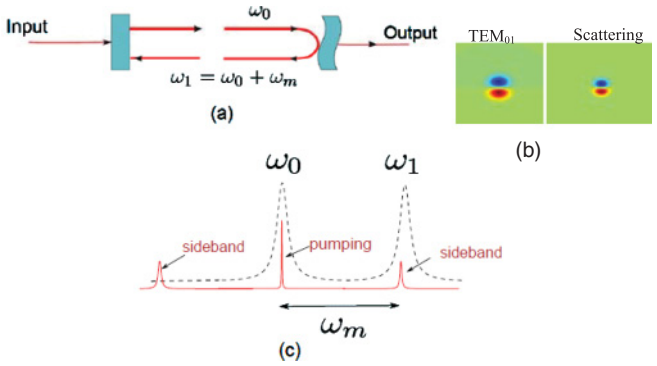

FIG. 1. (Color online) (a) Schematic of three-mode interaction in an optical cavity. Here, the anti-Stokes mode ω_1 has a similar mode shape to the internal acoustic mode of the end mirror and has a frequency of $\omega_1 = \omega_0 + \omega_m$. (b) Mode shapes of TEM$_{01}$ mode and optical mode scattered from the end mirrors. (c) Frequency structure of the two optical modes and sidebands. The laser is tuned to the fundamental TEM$_{00}$ mode with frequency ω_0. The mechanical motion induces two sidebands, but only one resonates in the high-order optical mode at ω_1 and gets amplified.

the Stokes mode) and the other at $\omega_0 + \omega_m$ (the anti-Stokes mode). With the correct frequency gap between the high-order mode at ω_1 and the fundamental mode (i.e., $|\omega_1 - \omega_0| = \omega_m$), one sideband mode (the anti-Stokes mode in the case shown in the figure) becomes resonant. If the mode-shape overlap is large, as defined by the overlap integral (discussed below) between the mode shape of the high-order mode and the mode shape of the acoustic mode, the optomechanical coupling can be large. The high-order mode carries the resonantly enhanced signal sideband. Because all the modes are resonant, high displacement sensitivity is achieved with relatively low optical power and sensitivity increases with cavity finesse. When correctly tuned, the optomechanical coupling and sensitivity scale as the product of two optical and one acoustic quality factor, all of which can be very large $\sim 10^6$ to 10^{10} [16]. This confers a large advantage compared with two-mode transducers.

It is interesting that the three-mode transducer is equivalent to the signal recycling configuration used for amplifying the signal sidebands in gravitational-wave detectors [23]. For the experiment described here, we used a TEM$_{01}$ mode for the second optical mode.

II. THREE-MODE OPTOMECHANICAL TRANSDUCER THEORY

The formalism for the three-mode interaction has been presented previously in general form in Refs. [22,23]. We summarize some of the results for the coherence of this paper. The three-mode interaction can be described by the following Hamiltonian:

$$\hat{\mathcal{H}} = \tfrac{1}{2}\hbar\omega_m\left(\hat{q}_m^2 + \hat{p}_m^2\right) + \hbar\omega_0\hat{a}^\dagger\hat{a} + \hbar\omega_1\hat{b}^\dagger\hat{b} + \hbar G_0\hat{q}_m(\hat{a}^\dagger\hat{b} + \hat{b}^\dagger\hat{a}) + \hat{\mathcal{H}}_{\rm ext}. \quad (1)$$

Here, $\hat{q}_m$ and $\hat{p}_m$ are the position and momentum of the mechanical mode, $\hat{a}$ and $\hat{b}$ are the annihilation operators for the fundamental optical cavity mode and the high-order optical cavity mode (the TEM$_{00}$ mode and the TEM$_{01}$ mode, respectively, in this experiment), $G_0 \equiv [\Lambda\hbar\omega_0\omega_1/(m\omega_m L^2)]^{1/2}$ is the optomechanical coupling constant with Λ representing the spatial overlap between the TEM$_{01}$ mode and the mechanical mode with m being the test mass mechanical mode effective mass and L being the cavity length, and $\hat{\mathcal{H}}_{\rm ext}$ is the coupling between the cavity modes and the injection external continuous mode $\hat{a}_{\rm in}$ and $\hat{b}_{\rm in}$ and is given by $\hat{\mathcal{H}}_{\rm ext} = i\hbar(\sqrt{2\gamma_0}\hat{a}^\dagger\hat{a}_{\rm in} + \sqrt{2\gamma_1}\hat{b}^\dagger\hat{b}_{\rm in} - {\rm H.c.})$ with γ_0 and γ_1 being the decay rates of the cavity modes and H.c. being the Hermitian conjugate.

From the above Hamiltonian, we can derive the equations of motion for the linearized dynamics (in the rotating frame at ω_0):

$$\ddot{\hat{q}}_m + 4\gamma_m\dot{\hat{q}}_m + \omega_m^2\hat{q}_m = \bar{G}_0(\hat{b} + \hat{b}^\dagger) + F_{\rm th} + F_{\rm sig}, \quad (2)$$

$$\dot{\hat{b}} + (\gamma_1 + i\Delta)\hat{b} = -i\bar{G}_0\hat{q}_m + \sqrt{2\gamma_1}\hat{b}_{\rm in}, \quad (3)$$

where $\Delta \equiv \omega_1 - \omega_0$, γ_m is the mechanical mode damping rate or the mechanical mode half linewidth, $\bar{G}_0 \equiv G_0\bar{a}$ where $\bar{a}$ is the zero-order intracavity intensity of mode TEM$_{00}$, $\hat{b}_{\rm in}$ is the vacuum fluctuation component in TEM$_{01}$ mode since there is no TEM$_{01}$ mode injected, $F_{\rm th}$ is the thermal Langevin force, and $F_{\rm sig}$ is the signal that we seek to probe. We neglect the intensity change of the TEM$_{00}$ mode, since it is almost constant and only determines the optomechanical interaction strength. The above linear dynamics can be easily solved and, from the standard input-output relation [24]

$$\hat{b}_{\rm in}(t) + \hat{b}_{\rm out}(t) = \sqrt{2\gamma_1}\hat{b}(t), \quad (4)$$

we can obtain the TEM$_{01}$-mode output $\hat{b}_{\rm out}(t)$ that we detect. In our experiment, which is described below, we detect the cavity transmission signal that includes the TEM$_{01}$ and TEM$_{00}$ modes. These modes beat at the quadrant photodetector (QPD) and give information on the TEM$_{01}$ mode. Because the TEM$_{00}$ mode is constant, by detecting the amplitude of the beating signal of the cavity transmission, we detect the amplitude quadrature $\hat{b}_1 = (\hat{b}_{\rm out} + \hat{b}_{\rm out}^\dagger)/\sqrt{2}$ of the TEM$_{01}$ mode. Ideally, if we can detect both the amplitude and phase quadratures, we can optimize the detection sensitivity since both quadratures contain information on the mechanical-mode amplitude. This can be done by introducing a local oscillator in the TEM$_{01}$ mode to beat with the cavity transmission. In the experiment reported here, where the sensitivity is still far from the standard quantum limit, we demonstrate high detection sensitivity with single-quadrature detection.

The displacement noise spectrum for the amplitude quadrature is [25],

$$S_{11}(\Omega) = \frac{\hbar Lc\left[(\Omega+\omega_m)^2 + \gamma_1^2\right]\left[(\Omega-\omega_m)^2 + \gamma_1^2\right]}{4\omega_0 I_0\gamma_1\omega_m^2} + \frac{\hbar\omega_0 I_0}{\gamma_1 Lc}|\chi|^2 + 4m\gamma_m k_B T|\chi|^2. \quad (5)$$

In Eq. (5), the first term is the quantum shot noise, the second term is the quantum radiation-pressure noise, and the last term is the thermal noise. Here, I_0 is the intracavity power for the TEM$_{00}$ mode, c is the speed of light, m is the effective test mass, γ_m is the mechanical mode linewidth, k_B is the Boltzmann constant, T is the environmental temperature, and $\chi(\Omega) = m[-(\Omega^2 - \omega_m^2) - i\gamma_m\Omega]^{-1}$ is the mechanical

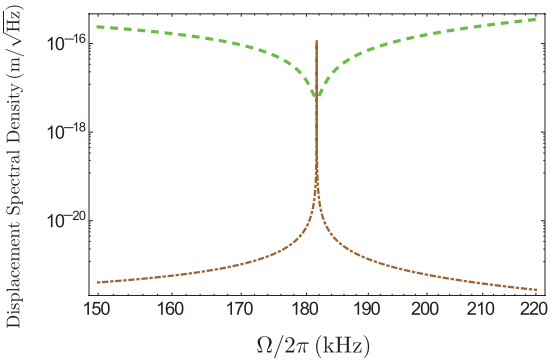

FIG. 2. (Color online) Theoretical displacement noise spectrum density. The dashed line shows the shot noise, the dash-dotted line shows the thermal noise, and the radiation-pressure noise is not shown because it is negligible. The parameters used are those for the experiment described in this paper.

response function. In the above calculation, we have ignored the correlation between the shot noise and the radiation-pressure noise, because the radiation-pressure noise is negligibly small in our experiment.

Figure 2 shows the quantum-limited noise spectral density (green dashed line) and the thermal noise at room temperature (black dash-dotted line). The parameters used for this figure are for the experimental setup described below and the quantum noise here is dominated by the shot noise. It can be seen from Eq. (5) that the shot noise term has a minimum when $\Omega = \omega_m$, which is at the three-mode resonance defined in Fig. 1. This is because the measurement shot noise at the QPD is constant at all frequencies but the signal sideband is coherently amplified by the TEM_{01} cavity resonance. This increases the signal-to-shot-noise ratio by the cavity resonance factor. At the optical power level used in the experiment described here the quantum backaction noise is still much smaller than the shot noise.

III. EXPERIMENTAL RESULTS

A 77 m high optical power cavity is used to investigate the three-mode interactions. The experimental setup is shown in Fig. 3. We use an Nd:YAG laser at a wavelength of 1064 nm. The laser is frequency locked to the 77 m Fabry-Pérot cavity. After passing through the mode-matching optics, the remaining optical power that enters the cavity is about 3.0 ± 0.3 W. With a cavity finesse of $1.3 \pm 0.1 \times 10^3$, the intracavity power is 300 ± 50 times as much as the input power, achieving almost 1 kW of circulating power.

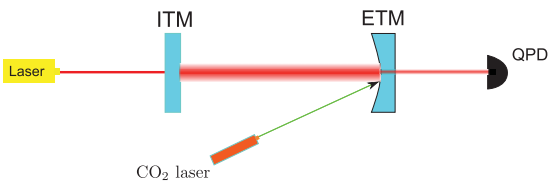

FIG. 3. (Color online) Thermal tuning radius of curvature of cavity end mirror for three-mode interaction using CO_2 laser heating and signal detection at cavity transmission using quadrant photodetector (QPD).

The original mode gap between TEM_{00} and TEM_{01} modes is ~201.6 kHz. In order to satisfy the resonant condition for the three-mode interaction, we need to tune the frequency gap between the TEM_{00} and TEM_{01} mode to match the mechanical-mode frequency. The frequency gap depends on the radius of curvature of the mirrors according to the following relation:

$$\omega_0 - \omega_1 = \frac{c}{L}\left[\arccos\sqrt{\left(1-\frac{L}{R_1}\right)\left(1-\frac{L}{R_2}\right)}\right]. \quad (6)$$

Here, R_1 and R_2 are the radii of curvature of the input test mass (ITM) and end test mass (ETM) mirrors, respectively.

This is achieved by thermally tuning the radius of curvature of test masses using CO_2 laser heating to create thermal deformation. Because the sapphire test mass has a high thermal conductivity, this thermal tuning is relatively fast. We can tune the radius of curvature by a few percent within seconds [28].

When the resonant conditions are satisfied and the spatial distribution of the sideband from the mechanical mode coincides with the TEM_{01} mode, the sideband signal will be enhanced by the cavity resonance. The amplitude quadrature of the TEM_{01} mode is proportional to the displacement of the ETM surface. The mixing between the TEM_{01} mode and the TEM_{00} mode creates a signal proportional to the test mass mechanical mode displacement. As the spatial profile of the TEM_{01} mode is antisymmetric, we use a quadrant photodiode (QPD) for differentially detecting the signal. This detection scheme has immunity to TEM_{00} noise because the differential detection cancels the common TEM_{00} noise and the high-finesse cavity is an excellent low-pass filter that reduces TEM_{00} noise at frequencies higher than the cavity linewidth. However, TEM_{01} noise, such as beam jitter noise, can still couple to the signal. An appropriate suspended mode cleaner [14] can reduce the TEM_{01} noise effectively but is not used in the current setup.

As we vary R_2 of the ETM by adjusting the CO_2 laser heating power we observe a high-Q-factor acoustic mode around 181.6 kHz. The amplitude of the signal is a function of the CO_2 heating power. We optimize the heating power to obtain maximum signal amplitude. In principle, the CO_2 heating also causes temperature-dependent changes of the mechanical mode resonance frequency. However, the maximum heating power used was less than 1 W and changes from this mechanism are less than those due to ambient temperature changes (demonstrated by simulation and experimental observation).

Figure 4 shows the QPD output signal as a function of the CO_2 heating power on the ETM. We can see clearly that there is an optimum heating power at which the mechanical sideband is enhanced by the cavity resonance.

The finite element simulation results show several acoustic modes near 181 kHz, but one particular mode has high overlap with the TEM_{01} mode and very small vibration amplitude at the suspension point, implying low losses into the suspension wires and high Q factor. The effective mass is 0.28 kg and the overlap with the TEM_{01} mode is 0.4, according to the simulation. This mode shape is shown in Fig. 5.

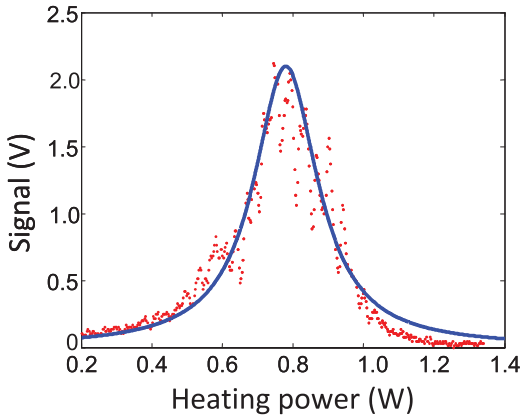

FIG. 4. (Color online) QPD signal at mechanical mode frequency as a function of CO_2 heating power. The black dots are the measured data; the blue solid line is the Lorentzian fit. The major fluctuations come from the fluctuation of suspended test-mass-mirror orientation due to seismic noise, since the auto-alignment system is difficult to implement with a thermally tuned cavity.

Figure 6 shows the signal spectrum at optimum heating power together with the theoretical prediction of the thermal noise and radiation-pressure noise (a zoom in of the top central part of Fig. 2).

To estimate the amplitude of the thermal noise, we use the theoretical value of the thermal noise spectrum, which from Eq. (5) can be expressed as

$$x^2 = 4m\gamma_m k_B T|\chi|^2 = \frac{4k_B T}{mQ\left[\left(\Omega^2-\omega_m^2\right)^2+\frac{\Omega^2}{Q^2}\right]}, \qquad (7)$$

where $Q=\omega_m/2\gamma_m$ is the mechanical quality factor of the test mass. We measured the Q factor of the mechanical mode by resonantly exciting the mode using an electrostatic actuator and recording the ringdown curve. From the ringdown curve we determined the Q factor for this particular mode to be $1.2\pm0.2\times10^6$. The three-mode interaction for this mechanical mode is in the regime of parametric cooling. However, the cooling factor is very small ($\sim10^{-2}$), so that the change of Q is only 1%, which is within the measurement

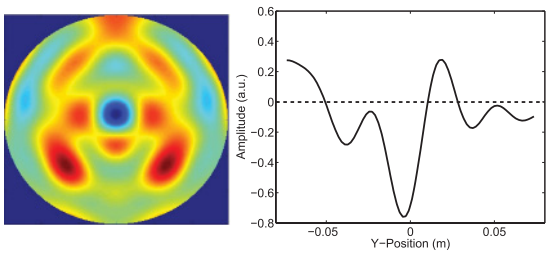

(a) (b)

FIG. 5. (Color online) Finite element model of the 181.6 kHz mechanical resonance of the test mass. (a) Two dimensional mode shape; (b) mode shape cross-section distribution along the center Y direction of the test mass. This model took into account the two flat surfaces at the circumference of the test mass and the crystalline anisotropy of the sapphire test mass (with different Young's moduli along different crystal axes).

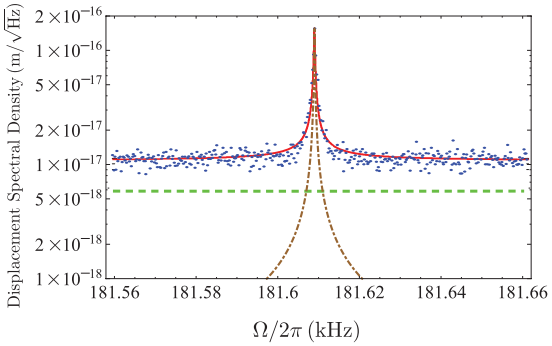

FIG. 6. (Color online) Experimental three-mode interaction spectrum. The dots show the measured data, which are fit by a Lorentzian curve (solid line). The dash-dotted line shows the calculated thermal noise spectrum; the dashed line shows the calculated shot noise.

uncertainty. Thus, this effect is not included in the theoretical thermal noise calculation.

The Lorentzian curve fit of the experimental peak in Fig. 6 gave a Q factor of $\sim 5\times10^5$, which is lower than the ringdown measurement. This is because the data shown in Fig. 6 is taken over several averages during which there is a slight frequency drift, causing broadening of the peak.

The temperature coefficient of resonance frequency change of sapphire is $\sim5\times10^{-5}$ Hz/K (depending on the crystalline axis) [26]. The heat capacity of sapphire [760 (J/K)/kg] ensures that frequency change during a typical measurement is less than the frequency resolution of the experiment of 0.6 Hz, which corresponds to a temperature change of the test mass of 65 mK. Thus, the thermal tuning has negligible effects on the test mass parameters except for the radius-of-curvature change that arises from surface expansion at the hot spot and the associated global-shape change of the test mass.

The total transmitted power on the QPD was measured to be about 4.0 ± 0.2 mW. To estimate the noise contribution to the QPD output, we blocked the cavity transmitted laser light and then illuminated it with a white light to create the same photocurrent. By comparing the QPD differential outputs with and without white light we determined the shot-noise level to be about half of the QPD electronic noise. Since the noise spectra are the same with both the cavity transmitted light and the white light on the QPD, we concluded that the transmitted laser light technical noise is negligible and is shot-noise limited at $\sim$181.6 kHz. The estimated radiation-pressure force that could drive the test mass internal mode motion is much smaller than the thermal noise. For this reason, we identify the resonance peak we measure as the thermal noise peak. By using the calculated thermal noise as a calibrator, we converted the measured data to the displacement noise spectrum as shown in Fig. 6. It should be noted that it is rather difficult to independently calibrate the thermal noise peak amplitude because cavity alignment fluctuations cause changes in the laser spot positions on the test mass, thereby causing fluctuations in the spatial overlap parameter Λ which determines the magnitude of the scattering between TEM_{00} and TEM_{01} modes.

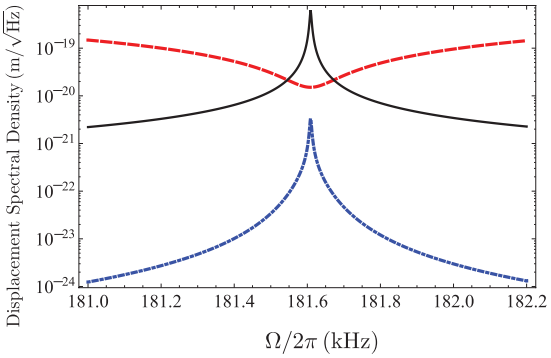

FIG. 7. (Color online) Expected achievable three-mode interaction sensitivity with improved cavity and photodetector (PD) parameters (cavity finesse 1500, ETM transmission 100 ppm, PD quantum efficiency 0.8). Solid line shows the thermal noise spectrum; dashed line shows the shot noise; dotted line shows the radiation-pressure noise.

We can see in Fig. 6 that the noise level off resonance is $\sim 10^{-17}$ m/$\sqrt{\text{Hz}}$, limited mainly by the sum of photodetector electronic noise and quantum shot noise. The sensitivity of this experiment can be improved in a straightforward fashion by increasing the cavity finesse, the ETM transmissivity, and the photodetector's quantum efficiency, as well as to add a suspended mode cleaner to filter out high-order modes before the cavity injection. Figure 7 shows the calculated thermal noise, the shot noise and the radiation-pressure noise of the system with a cavity finesse of 15 000 (achievable with typical commercially available good quality mirrors), ETM transmission of 100 ppm, QPD quantum efficiency of 0.8 [27], input power of 5 W, and the same mechanical parameters as in the current experiment. The three-mode parametric cooling effect is obvious in Fig. 7, as shown by the increased acoustic mode linewidth. The thermal noise is still the dominated noise near the resonance. The quantum shot noise limits the off-resonance sensitivity. The best displacement sensitivity achievable is close to 2×10^{-20} m/$\sqrt{\text{Hz}}$.

IV. CONCLUSIONS

In conclusion, we have demonstrated the intrinsic high sensitivity of a three-mode opto-acoustic parametric transducer. The measurement scheme has intrinsic immunity to laser amplitude and phase noise. The technique has applications to ground-state cooling of kilogram-scale test masses, quantum nondemolition measurements, measurement of radiation-pressure noise, and to the precision monitoring of test mass modes in gravitational-wave detectors.

ACKNOWLEDGMENTS

This research was supported by the Australian Research Council and the Western Australian government Centres of Excellence. We would like to thank the LIGO Scientific Collaboration and Gingin International Advisory Committee, especially, Stefan Goßler, Gregg Harry, Bill Kells, and Phil Willems for useful discussions, and Pierre-François Cohadan and Antoine Heidmann for collaboration on small-scale three-mode devices.

[1] V. B. Braginsky and F. Ya. Khalili, *Quantum Measurement* (Cambridge University Press, Cambridge, 1992).
[2] T. J. Kippenberg and K. J. Vahala, Science **321**, 1172 (2008); F. Marquardt and S. M. Girvin, Physics **2**, 40 (2009).
[3] D. Vitali, S. Gigan, A. Ferreira, H. R. Böhm, P. Tombesi, A. Guerreiro, V. Vedral, A. Zeilinger, and M. Aspelmeyer, Phys. Rev. Lett. **98**, 030405 (2007).
[4] M. Paternostro, D. Vitali, S. Gigan, M. S. Kim, C. Brukner, J. Eisert, and M. Aspelmeyer, Phys. Rev. Lett. **99**, 250401 (2007).
[5] H. Müller-Ebhardt, H. Rehbein, R. Schnabel, K. Danzmann, and Y. Chen, Phys. Rev. Lett. **100**, 013601 (2008).
[6] M. J. Hartmann and M. B. Plenio, Phys. Rev. Lett. **101**, 200503 (2008).
[7] J. Thompson, B. Zwickl, A. Jayich, F. Marquardt, S. Girvin, and J. Harris, Nature (London) **452**, 72 (2008).
[8] H. Miao, S. Danilishin, T. Corbitt, and Y. Chen, Phys. Rev. Lett. **103**, 100402 (2009).
[9] J. D. Teufel, T. Donner, Dale Li, J. W. Harlow, M. S. Allman, K. Cicak, A. J. Sirois, J. D. Whittaker, K. W. Lehnert, and R. W. Simmonds, Nature (London) **475**, 359 (2011).
[10] LIGO project Web site [http://www.ligo.caltech.edu].
[11] VIRGO project Web site [http://www.virgo.infn.it/].
[12] O. Arcizet, P.-F. Cohadon, T. Briant, M. Pinard, A. Heidmann, J.-M. Mackowski, C. Michel, L. Pinard, O. Français, and L. Rousseau, Phys. Rev. Lett. **97**, 133601 (2006).
[13] B. Abbott *et al.*, New J. Phys. **11**, 073032 (2009).
[14] B. P. Abbott *et al.*, Rep. Prog. Phys. **72**, 076901 (2009).
[15] William E. Butler, Ph.D. thesis (unpublished), University of Rochester, 2004.
[16] C. Zhao, L. Ju, H. Miao, S. Gras, Y. Fan, and D. Blair, Phys. Rev. Lett. **102**, 243902 (2009).
[17] V. B. Braginsky *et al.*, Phys. Lett. A **287**, 331 (2001); **293**, 228 (2002); **305**, 111 (2002).
[18] C. Zhao, L. Ju, J. Degallaix, S. Gras, and D. G. Blair, Phys. Rev. Lett. **94**, 121102 (2005).
[19] S. Gras, C. Zhao, D. G. Blair, and L. Ju, Class. Quantum Grav. **27**, 205019 (2010).
[20] H. S. Bantilan and W. Kells, *Investigating a Parametric Instability in the LIGO Test Masses* (LIGO Document: LIGO-T060207-00-Z).
[21] S. E. Strigin, D. G. Blair, S. Gras, and S. P. Vyatchanin, Phys. Lett. A **372**, 5727 (2008).
[22] J. M. Dobrindt and T. J. Kippenberg, Phys. Rev. Lett. **104**, 033901 (2010).
[23] H. Miao, C. Zhao, L. Ju, and D. G. Blair, Phys. Rev. A **79**, 063801 (2009).

[24] D. F. Walls and G. J. Milburn, *Quantum Optics* (Springer-Verlag, Berlin, 1994).

[25] Haixing Miao, Stefan Danilishin, Helge Müller-Ebhardt, and Yanbei Chen, New J. Phys. **12**, 083032 (2010).

[26] D. P. Tsarapkin, *Frequency Control Symposium, 1994. 48th., Proceedings of the 1994 IEEE International* (IEEE, Boston, MA,1994), pp. 451–458.

[27] K. Goda *et al.*, Nature Phys. **4**, 472 (2008).

[28] C. Zhao *et al.*, Phys. Rev. Lett. **96**, 231101 (2006).